High occurrence of new particle formation events at the Maïdo high altitude observatory (2150 m), Reunion Island (Indian Ocean)

Brice Foucart[1, 2], Karine Sellegri[2], Pierre Tulet[1], Clémence Rose[2], Jean-Marc Metzger[3], and David Picard[2]

[1]Laboratoire de l'Atmosphère et des Cyclones (LACy-UMR 8015, CNRS, Université de La Réunion, Météo-France), 97744 Saint Denis de La Réunion, France.
[2]Laboratoire de Météorologie Physique (LaMP-UMR 6016, CNRS, Université Blaise Pascal), 63178, Aubière, France.
[3]Observatoire des Sciences de l'Univers de La Réunion, UMS 3365 (CNRS, Université de La Réunion), 97744 Saint Denis de La Réunion, France.

Correspondence to: Brice Foucart (brice.foucart@univ-reunion.fr)

Abstract. This study aims to report and characterize the frequent new particle formation (NPF) events observed at the Maïdo observatory, Reunion Island, a Southern Hemisphere site located at 2150 m and surrounded by the Indian Ocean. In 2014 and 2015, continuous aerosol measurements were made using both a Differential Mobility Particle Sizer (DMPS) and an Air Ion Spectrometer (AIS) to characterize the NPF events down to the lowest particle size scale. Carbon monoxide (CO) and sulfur dioxide (SO_2) concentrations were monitored, as well as meteorological parameters, in order to identify the conditions that were favourable to the occurrence of nucleation in this specific environment. We point out that the annual NPF frequency average (65%) is one of the highest reported so far. Monthly averages show a bimodal variation of the NPF frequency, with a maximum observed during off-season periods (March to May and September to December). A high yearly median particle Growth Rate (GR) of 15.16 nm.h^{-1} is also measured, occasionally peaking at values of the order of 100 nm.h^{-1} and showing a bimodal seasonal variation with maxima observed in July and November. Yearly medians of 2 and 12 nm particle formation rates (J_2 and J_{12}) are 0.858 and 0.508 cm^{-3}.s^{-1} respectively, with a seasonal variation similar to that of the GR. The seasonal variations of GR and J correspond to the seasonal variation of radiation, which may be responsible for more efficient photochemistry and also for a higher influence of the boundary layer, as shown by the CO seasonal variation. Multiple sources can contribute to the NPF frequency and intensity, including marine, biogenic from vegetation, and anthropogenic sources.

1 Introduction

Aerosol concentrations in the atmosphere influence the Earth's radiative balance, and the formation and lifetime of clouds (Seinfeld and Pandis, 2016; Makkonen et al., 2012). Unlike the primary sources of aerosols, such as soil erosion, sea salt, and volcanic ash, nucleation is a gas-to-particle conversion process leading to the formation of new secondary aerosol particles. Nucleation and subsequent growth are responsible for New Particle Formation (NPF) events, observed in various environments around the world (Kulmala et al., 2004) but still rarely in the southern hemisphere. The frequency, intensity and duration of NPF events is highly variable according to the location where they are observed. The occurrence and characteristics of NPF episodes depend on various factors, including the emission strength of precursors, the number concentration of the pre-existing aerosol population, and

meteorological parameters (in particular solar radiation, temperature and relative humidity), which directly influence photo-chemical processes (Kulmala, 2003; Martin et al., 2010; Hallar et al., 2016). However, the

40 relationship between these environmental parameters and the characteristics of NPF events is not fully understood and it is still a challenge to predict when an NPF event will take place and how intense it will be (Kulmala et al., 2004; Yu et al., 2008). Consequently, there is still a need to report and describe NPF in environments that have not yet been investigated, notably in the Southern Hemisphere in general and more particularly for both marine and high altitude tropical sites. These kinds of environments present true specificity in terms of RH variability,

45 emission types (VOCs and Marine sources) and atmospheric dynamics. Previous studies that have been conducted in the Southern Hemisphere relate to South Africa (Hirsikko et al., 2012), which is both a low latitude and a medium altitude (1400 m) site, South America (Rose et al., 2015a) and Australia (Bates et al., 1998), which are medium latitude, and Antarctica (Koponen et al., 2003) as a high latitude area. Hirsikko et al. (2012) published the highest NPF frequency ever reported, of about 86%, explaining that both the local sources (strong mining

50 pollution) and regional conditions affected the NPF variation. Recently, Rose et al. (2015a) proposed a low-latitude zone analysis of NPF at Chacaltaya (CHC) in Bolivia, which is one of the highest in situ measurement sites in the world (5240 m). They, too, found a very high NPF frequency, of about 63.9%. This value has been partly explained by lower concentrations of pre-existing particles than at lower altitudes, leading to smaller loss of gaseous precursors, while photochemical activity is enhanced by higher radiation. In addition, at high altitude stations,

55 turbulence at the interface between the Boundary Layer (BL) and the Free Troposphere (FT) might promote nucleation and growth processes (Hamburger et al., 2011). In general, high altitude sites report relatively high NPF event frequencies, such as 35% at Nepal Climate Observatory (5079 m; Venzac et al., 2008) or 35.9% at the Puy de Dôme station (1465 m; Boulon et al., 2011a).

Reunion Island, which is located at low latitude in an inter-tropical area surrounded by the Indian Ocean, is still

60 poorly documented. The island, which was partly shaped by the active basaltic volcano of Piton de la Fournaise (PdF), is characterized by angular landforms and steep slopes. The interaction of the high mountainous terrain with the synoptic flow induces large variability in wind fields at local scale. The maritime and tropical location of the island combined with the complexity of the terrain and wind exposure implies a multitude of local circulations and weather, marked by large variations in temperature and precipitation. This complex atmospheric dynamics added

65 to a large variety of primary and secondary NPF sources (marine, organic and anthropogenic) gives special interest to this study. The Maïdo observatory is located at 2200 m a.s.l., under the influence of the marine boundary layer during daytime and of the free troposphere during night-time (Tulet et al., 2017). The main objective of this study is to reinforce the observations of NPF events in the Southern Hemisphere and more particularly for a site that is both marine and at altitude. We first describe how NPF was observed at the site by DMPS and AIS interpolation

70 (Sect. 4.1.). Based on a multiyear data set of clusters and aerosol size distributions, we secondly report the frequency (Sect. 4.2.), the intensity (Sect. 4.3.) and the characteristics of the events, and describe their seasonality. Thirdly, we analyse their annual variations with respect to the meteorological parameters (Sect. 4.4) and the pre-existing particle concentration (Sect. 4.5.).

2 Characteristics of the Maïdo observatory

2.1 Geographical location and networks

Maïdo observatory (21.080° S 55.383° E) is situated on La Reunion Island in the Indian Ocean. There are very few multi-instrumented stations in the tropics, and particularly in the southern hemisphere (Baray et al., 2013), so the Maïdo observatory was built in 2012 to respond to the needs of major international networks like NDACC (Network for the Detection of Atmospheric Composition Change, http://www.ndacc.org) and ACTRIS (Aerosols, Clouds, and Trace gases Research Infra-Structure network). It is a high-altitude station (2150 m), which opens up new perspectives in upper troposphere and lower stratosphere studies. Belonging to the Global Atmosphere Watch regional network (GAW), it also conducts in situ measurements to characterize the atmospheric composition of the lower troposphere. The facility dominates, in the east, the natural amphitheatre of Mafate, characterized by lush tropical vegetation, and, in the west, the highland tamarind forests. The nearest urban areas are the coastal cities of Saint Paul and Le Port with 105.000 and 40.000 inhabitants respectively, located 13 and 15 km away from the Maïdo observatory (Fig. 1).

2.2 Large and local scale atmospheric dynamics

At a large scale, the island is located in the descending part of the South Hadley cell (Baldy et al., 1996). It is subject to the intertropical zone atmospheric circulation, which is characterized by a trade wind flow from the south-east in this lower layer, induced by the Hadley cell and accentuated by more zonal driving by the Walker circulation. This lower layer flow is limited in altitude (about 3 km) by westerly winds (westerlies), which constitute the return of the Hadley – Walker circulation. In terms of rainfall, Reunion Island is characterized by two seasons: the hot, wet season from January to March (southern summer) and the cold, dry season (southern winter), which is longer, lasting from May to November (Baray et al., 2013). April and December are transition months that can be rainy or dry. In the southern summer, the Inter-Tropical Convergence Zone (ITCZ) is situated in the southern hemisphere and sometimes reaches Reunion Island. The westerly flow (between 30°N and 30°S) and west winds weaken and are strongly affected by the context of heavy rains. During the southern winter, the subtropical high pressures are more powerful than during the southern summer and maintain the synoptic subsidence (descending branch of the Hadley cell) that generates and feeds the stream of faster moving trade winds on the Mascarene region.

On a local scale, it is possible to observe two major atmospheric phenomena on both sides of the island. Trade winds coming from the south-east are separated (Fig.1) by the high topography of Reunion, which acts as an obstacle (Lesouëf et al., 2011). They are confined under the inversion layer and forced to bypass the island, forming two branches (Soler, 2000). During the day, a returning loop (Fig. 1) forms in the north-east when the winds converge. The inversion of the circulation then brings the winds under the cities of Saint Paul and Le Port up to the heights towards the Maïdo station. Moreover, the interaction between the trade winds and the abrupt relief of Reunion creates strong climate asymmetry and many microclimates. The warming of mountain slopes by solar radiation during the day, or radiative cooling overnight, is transmitted to the surrounding air layers and creates a complex local circulation. The nocturnal surface radiative cooling induces a cold katabatic wind on the slopes and clears the atmosphere at the Maïdo station, leaving the observatory in the free troposphere, disconnected from the anthropogenic pollution. Thus there are few clouds during the night-time. After midday, the sea breeze cumulated

in the returning loop wind direction generates upward winds on the slopes which transport particles to the high station, accompanied by orographic and slope cloud formation. The surface radiative warming tends to create convection and then form vertical clouds located at the top of the relief. The number of nights with clear sky is

115   then very large in comparison with the coastal site of Saint Denis, where LIDARs were operated from 1994 to 2011 (Baray et al., 2013).

2.3 Potential gas-phase precursor sources

The different environments that are present at local scale (Fig. 1) can correspond to different types of gas-phase precursor sources, each having different seasonal variations that can be investigated.

120   **2.3.1 Sulfur dioxide (SO$_2$) and sulfuric acid (H$_2$SO$_4$)**

Several studies have provided evidence that high SO$_2$ concentrations and high radiation levels favour the formation of large amounts of H$_2$SO$_4$, which in turn contribute to particle formation (Hyvönen et al., 2005; Mikkonen et al., 2006; Petäjä et al., 2009) and growth (Boy et al., 2005; Sihto et al., 2006; Mikkonen et al., 2011). Except for some altitude cases where the role of sulfuric acid in nucleation is limited (Boulon et al., 2011a; Rose et al., 2015a;

125   Bianchi et al., 2016), H$_2$SO$_4$ is thought to be among the major precursors of NPF due to its low saturating vapour pressure under conventional atmospheric temperature conditions (Kulmala and Kerminen, 2008). The Maïdo observatory can be on the pathway of sporadic SO$_2$ volcanic plumes emitted from the Piton de la Fournaise (PdF) volcano, located in the south of the island (Fig 1). In 2015, four eruptions where observed (Peltier et al., 2016) and multidisciplinary tracking of a volcanic gas and aerosol plume was conducted by Tulet et al., 2017.

130   Unfortunately, H$_2$SO$_4$ was not measured but their results indicated that the Maïdo station was reached by the plume several times, as evidenced by the detection of SO$_2$ concentration peaks (Fig. A1). Specifically in a volcanic plume environment, Boulon et al. (2011b) directly observed NPF events within the Eyjafjallajökull volcanic plume that reached the Puy de Dôme station, and related them to the presence of high H$_2$SO$_4$ concentrations. During the PdF eruption that took place in April 2007, Tulet and Villeneuve (2011) used OMI and CALIOP space sensor data to

135   estimate a total SO$_2$ release of 230 kt, 60 kt of which was transformed into H$_2$SO$_4$, mostly above the Indian ocean, at 6 km a.s.l. As a first analysis, we focus on the parameters influencing new particle formation (NPF) processes at the Maïdo station outside the very specific conditions encountered during a volcanic plume advection, which will be the topic of a separate study. Data were therefore screened for the presence of the Piton de la Fournaise plume at the station. The volcanic plume was considered to be present when the SO$_2$ concentration reached values

140   higher than 1 ppb (hourly average), which is the 97th percentile estimated on non-eruptive days. According to Boulon et al. (2011b), this threshold also represented a lower limit of the presence of the plume at the Puy de Dôme station. Consequently, 47 daytime plume days that occurred during three eruptive periods (Fig. A1) were listed and removed from the 2015 data set. In addition to volcano eruptions, the major causes of SO$_2$ emissions are connected with human activities: agriculture, power plants, sugar exploitation and road traffic. Because of the

145   relief of the island, urbanized areas are mostly located on the coast (Fig. 1). Reunion has a relatively developed urban fabric with eight cities having over 30.000 residents. For several decades population growth has been strong and urban pollution has increased in consequence.

2.3.2 Ammonia (NH₃) and amines

Ammonia can act as a stabilizing chemical base for H_2SO_4 in ternary nucleation theory. NH_3 can be derived from
150   chemical fertilizers, industrial (Ge et al., 2011) and especially bovine waste (Hutchinson et al., 1982; Schade and
Crutzen, 1995), decomposition of organic matter in the soil by certain bacteria (Gale, 1940) and biomass
combustion. Agriculture occupies 10% of the working population of Reunion and agricultural territory covers 20%
of the island (National Institute of Statistical Economic Studies, INSEE, 2017) mostly on gentle slopes (Fig. 1).
Consequently, there are potential sources of ammonia that could influence the observations at the Maïdo
155   observatory but we are not able to verify their existence because no direct measurements have been made. Amines
originating from the alkylation of ammonia can be found in the atmosphere in the primary, secondary or tertiary
state. For a time, significant concentrations of dimethylamine detected during the formation of nanoparticles in a
natural atmosphere suggested that alkylamines could contribute to the formation and growth of new particles
(Sellegri et al., 2006; Smith et al., 2010). Recently, it has been shown that amines have some weight in the
160   calculation of nucleation rates since they act as strong bases and are at the origin of clusters that are more stable
and more resistant to evaporation (Almeida et al., 2013).

2.3.3 Volatile Organic Components (VOCs)

Several studies have shown that oxidized monoterpenes can act as precursors of NPF events (Kulmala et al., 2013;
Schobesberger et al., 2013; Ehn et al., 2014). In 2014, the CLOUD experiment performed at CERN confirmed that
165   oxidation products of biogenic emissions could contribute to the nucleation of atmospheric particles (Riccobono
et al., 2014). Plants are able to emit biosynthesized Volatile Organic Compounds (VOCs) into the atmosphere
(Kesselmeier and Staudt, 1999), such as terpenes, which govern the correlation between sulfuric acid concentration
and new particle formations (Bonn et al., 2008). The H_2SO_4-Organics nucleation strongly depends on temperature
variation according to (Yu et al., 2017). Furthermore, (Kirkby et al., 2016) also show that α-Pinene oxidation
170   products can nucleate without sulfuric acid. As mentioned earlier, the Maïdo observatory is located above the
caldera and at the top of the steep slopes characterized by dense, specific tropical vegetation (Fig. 1). In order to
study the interactions between forests, gases, aerosols and clouds, the BIO-MAÏDO campaign took place in 2015
(Duflot et al., in prep) to obtain further information about the transport and chemical transformation of biogenic
compounds at the Maïdo observatory.

175   2.3.4 Phytoplankton

Using semi controlled seawater-air enclosures, Sellegri et al. (2016) presented evidence that nucleation may occur
from marine biological emissions in the open Mediterranean Sea. They identified iodine-containing species as
major precursors for the formation of new particle clusters. They also found a significant correlation between
iodine-containing species and some phytoplanktonic pigments (peridinin, chlorophyll b, and zeaxanthin) but not
180   with the total autotrophic biomass (Chl a). There is seasonal and spatial variability in phytoplankton biomass in
the north-western Indian Ocean (Veldhuis et al., 1997) and more particularly on the Somalian coast during a strong
upwelling that occurred between 7°N and 11°N in July. Although the Indian Ocean is an oligotrophic ocean, the
coasts of Reunion are sometimes subject to small phytoplanktonic blooms after severe rainfall periods, which
warm the water and produce upwellings. It also appears that, during the southern winter, the island has already

185 been on the pathway of the nutriment plume of the Indian Ocean gyre, which is composed of both the South

Equatorial and the West Australian Currents (Turquet et al., 2008)

2.3.4 Biomass burning

Due to its location, Reunion Island is seasonally exposed to biomass burning plumes from the African continent

and Madagascar, which can significantly affect the free tropospheric concentrations of ozone (Clain et al., 2009)

190 and other pollutants like carbon monoxide and several volatile organic compounds (Duflot et al., 2010; Vigouroux

et al., 2012). This kind of event can either inhibit or stimulate the nucleation process. Primary particulate pollutants

are compounded by the emission of high levels of secondary aerosol precursors, including oxides of nitrogen and

sulfur, volatile carbon species, and ammonia, resulting in the production of large amounts of secondary inorganic

and organic aerosols (Rastogi et al., 2014). The organic ones could be oxidized and act as a gas precursor whereas

195 pollutants can be considered as pre-existing particles and can prevent new particles from forming. In 2015, the

carbon monoxide variation seems to show a typical signature of such pollution events at Maïdo observatory (Fig.

2). The annual average concentration is about 63.7 ppb and the lowest value is 27.7 ppb, recorded on 02 February,

whereas the highest is 141.4 ppb attributed to 04 September (daily averaged). It clearly appears that there is an

increasing trend from May to December. Concentration peaks exceeding 0.8 ppm are visible in August, September,

200 October and November and can be compared to the tropospheric ozone (O_3) content variation observed by Taupin

et al. (1999), who recorded high values from August to December with peaks in October as observed by

Randriambelo et al. (1997), which correspond to biomass burning plumes from Madagascar or from South Africa.

2.4 Instrumentation used

The aerosol and ion size distributions used in the present study were measured continuously from 01 January to

205 31 December 2015 at the Maïdo observatory. The size distribution of the 10-500 nm aerosol particles was

measured with a Differential Mobility Particle Sizer (DMPS) while the size distribution of the 0.8-42 nm ions was

measured with an Air Ion Spectrometer (AIS). Here we use ion size distributions below 10 nm as tracers for the

presence of neutral sub-10 nm particles that could not be detected directly. Additional DMPS measurements

conducted between May and December 2014 will also be discussed briefly in section 4.1 to evaluate the inter-

210 annual variability of the nucleation frequency.

The DMPS was custom-built with a TSI-type Differential Mobility Analyzer (DMA) operating in a closed loop

and a Condensation Particle Counter (CPC, TSI model 3010). Particles were charged to equilibrium using an Ni-

63 bipolar charger at 95 MBq. The quality of the DMPS measurements was checked for flow rates and RH

according to the ACTRIS recommendations (Wiedensohler et al., 2012). DMPS measurements were performed

215 down a Whole Air Inlet with a higher size cut-off of 25 µm (under average wind speed conditions of 4 m.s^{-1}).

The AIS was developed by Airel, Estonia, for in situ high time resolution measurements of ions and charged

particles (Mäkelä et al., 1996). The device consists of two DMA arranged in parallel, which allows the

simultaneous measurement of both negatively and positively charged particles. Each of the two analysers operates

with a total flow of 90 litres per minute (lpm): 30 lpm of air to be sampled and 60 lpm of clean air (or carrier gas)

220 circulating in closed loop. The AIS was directly connected to ambient air through a 30 cm long copper inlet 2.5

cm in diameter, to limit cluster ion losses along the sampling line. The AIS measurements allowed the growth rate

of newly formed particles to be calculated from their lowest sizes (Hirsikko et al., 2005).

The global radiation was measured using a Sunshine Pyranometer (SPN1, Delta-T Devices Ltd.) with a resolution of 0.6 W.m⁻². The auxiliary measurements used in the present study were the wind direction, the wind speed, the

225 air temperature, the barometric pressure and the relative humidity. They were measured using the Vaisala Weather Transmitter WXT510 (http://www.vaisala.com).

The analyser used to measure sulfur dioxide (SO_2) concentrations uses the ultraviolet fluorescence method, standard NF EN 14212. The molecules are excited under the action of intense, constant UV radiation (214 nm). Sulfur dioxide then de-energizes very quickly by emitting higher wavelength radiation (between 320 and 380 nm)

230 than the excitation step. SO_2 concentration was finally calculated by means of a photomultiplier. Datasets were provided by the Observatoire Réunionnais de l'Air (ORA). The SO_2 analyser resolution was about 0.5 ppb and, outside eruptive periods, it never exceeded this threshold (Fig. A1). The corresponding data were used only to list days that were characterized by the presence of the volcanic plume at the Maïdo observatory.

CO monitoring was performed using a PICARRO G2401 analyzer which is compliant with international ambient

235 atmospheric monitoring networks, including the World Meteorological Organization (WMO) and the Integrated Carbon Observation System (ICOS, https://www.icos-ri.eu/). It was the property of BIRA-IASB (Belgian Institute for Space Aeronomy).

Figure 3 shows the availability of data for the main aerosol and gas-phase parameters used in this study. The best instrument synchronization period was from May to November.

240 **3 Calculations**

The classification of event days was achieved visually using the contour plot of the DMPS size distribution. The positive and negative ion size distributions provided by the AIS confirmed the status of the event when available. Days were classified and separated into three main groups: undefined, (UN) non-event (NE) and event (E) days according to Dal Maso et al. (2005).

245 The monthly event frequency, f_m, was calculated as the ratio of event to non-event days, after having excluded undefined, missing and plume days (PD), according to Eq. (1):

$$f_m = \frac{number\ of\ E}{number\ of\ days\ in\ month - (missing\ data\ days + PD)} \times 100 \ , \tag{1}$$

The condensation sink (CS; s⁻¹), which represents the loss rate of vapours on pre-existing particles was calculated from the DMPS size distributions according to Pirjola et al.'s (1999) Equation (2):

250
$$CS = 4\pi D_{vap} \int_0^\infty r\beta(r)N(r)dr \tag{2}$$

where D_{vap} is the condensable vapour diffusion coefficient, r the particle radius and $N(r)$ the concentration of particles of radius r. Coefficient $\beta(r)$ was calculated from the Knudsen number and is given by Eq. (3):

$$\beta(r) = \frac{1+Kn(r)}{1+Kn(r)\left(\frac{4}{3\alpha}+0.337\right)+\frac{4}{3\alpha}Kn(r)^2} \tag{3}$$

where $Kn(r)$ is the Knudsen number given by $Kn(r) = \lambda / r$, with λ corresponding to the particle free path

255 (depending on pressure and temperature) and the accommodation coefficient α, usually set at 1. The condensation sink was calculated with a five minute time resolution. As the particles are drained in the DMPS, we are aware that the CS, which depends on the diameter of wet particles, was underestimated.

The particle growth rate (GR; nm.h⁻¹) was determined using the "maxima" method of Hirsikko et al. (2005). The method searches, usually over the AIS channel size, for the time that corresponds to the maximum concentration

260 in each size channel. We applied the method to the DMPS 12-19 nm size range because the DMPS offers a much more extended data set than the AIS. In order to detect the concentration maximum, a normal distribution was fitted to the time evolution of the concentration for each channel. GR corresponded to the slope of the linear regression on the time-diameter pairs.

The formation rate of 12 nm particles, J_{12}, (cm⁻³.s⁻¹) was calculated using the following Equation (4) given by

265 Kulmala et al. (2007):

$$J_{12} = \frac{dN_{12-19}}{dt} + CoagS_{12} \times N_{12-19} + \frac{7}{1\ nm} \times GR_{12-19} \times N_{12-19} \tag{4}$$

where N_{12-19} is the concentration corresponding to 12 to 19 nm particle diameters, $CoagS_{12}$ represents the coagulation of 12 nm particles on pre-existing larger diameter particles and GR_{12-19} corresponds to the growth rate estimated between 12 and 19 nm. It was then possible to derive the nucleation rates of particles 2 nm in size,

270 J_2, from the J_{12} previously calculated from DMPS and the growth rate of particles between 2 and 12 nm, following the method first introduced by Kerminen and Kulmala (2002) and improved by Lehtinen et al. (2007) with Eq. (5):

$$J_2 = \frac{J_{12}}{\exp\left(-\gamma \times d_1 \times \frac{CoagS_{(d_2)}}{GR_{12-19}}\right)} \tag{5}$$

where,

$$\gamma = \frac{1}{m+1}\left[\left(\frac{d_{12}}{d_2}\right)^{m+1} - 1\right] \tag{6}$$

275 and,

$$m = \frac{\log\left(CoagS_{(d_{12})}\right) - \log\left(CoagS_{(d_2)}\right)}{\log(d_{12}) - \log(d_2)} \tag{7}$$

4 Results and discussion

4.1 DMPS and AIS data merging

A temporal interpolation was first performed to harmonize the DMPS and the AIS data sets to a 5 min resolution.

280 The AIS covers the size range between 0.90 and 46.2 nm while the DMPS covers the size range between 11.78 and 706.77 nm. For visual inspection of the consistency of the two data sets, hybrid plots were drawn up showing the AIS negative ion concentration up to 12 nm and then the particle concentration from the DMPS for larger sizes. Figure 4 shows an example of an NPF event followed by the two devices on 28 August, 2015. Typically, NPF events observed at the Maïdo observatory show an increase of small ion concentrations (2-5 nm) at dawn (04:00

285 UTC, corresponding to 08:00 LT). These small ions are tracers for small particles of the same size that rapidly grow to the first DMPS size classes within the next hour. The initiation of the formation of new particles at 04:00 UTC (08:00 LT) is accompanied by the appearance of accumulation mode particles. We suppose that this is due to a local emission that we are not able to able to determine yet. Further growth of the newly formed particles is generally accompanied by the simultaneous growth of the accumulation mode particles, starting around 07:00

290 UTC (11:00 LT). At the end of the afternoon, the accumulation mode particles are no longer detected at the station,

and a night-time Aitken mode becomes predominant. These particles are probably present in the free troposphere and are sampled at the site in subsiding air masses (Tulet et al., 2017).

4.2 Nucleation and frequency analysis

Over the measurement period in 2015, 47 volcanic plume days were excluded and data was missing on 61 days.

295   Among the 257 remaining days, 167 days (65%) were classified as event days, 55 (21%) as non-event days and 35 (14%) as undefined. As a result, the event frequency was high for the Maïdo station, with an annual average of 65% (med: 65.2%; 25ile: 52.0%; 75ile: 80.0%) for 2015. This frequency is one of the highest values reported so far, with the exceptions of the South African plateau, where NPF was reported to occur 86% of the time according to (Hirsikko et al., 2012), and savannah, with 83% of the time (Vakkari et al., 2011). Figure 5 shows the seasonal

300   variation of the monthly event frequency, f_m.

High NPF frequencies were observed during the austral off-season periods (around the transition months) being on average 72.5% for October and November, and even slightly higher, 89.4%, for March to May (Fig. 5). Note that continuous DMPS spectra of April (93.1% occ.) and June (46.7% occ.) are available in the appendices section though Figure A3. At the beginning of the southern winter and summer seasons (from June to August and from

305   January to February), NPF was lower. As shown in Figure 5, similar seasonal trends were observed for the nucleation frequency in 2014 and 2015. NPF was, on average, more frequent between September and December, while it was less frequent between May and August in 2014, with the highest inter-annual variability observed in May. Frequency variation does not appear to be governed by the dry or the wet periods (shown in Fig. 9b) and we observed both high and low frequency averages for both of them. These results are in contrast with those reported

310   by Rose et al. (2015a) for the CHC station, Bolivia, 5200 m above sea level. They reported high NPF frequencies during the southern winter. Because of a lack of knowledge about the potential gas precursor variation at Reunion Island, it is quite difficult to explain the event frequency variation with respect to the sources. However, we can say that the Somalian phytoplankton bloom, which generally occurs in July, does not seem to positively influence the frequency average for this month. In contrast, the CO variation has peaks in September, November and

315   December and is correlated with high event frequency averages during this period, but does not explain high NPF frequency in the period from March to May.

4.3 Particle formation, growth and nucleation rates

The yearly average particle growth rate for 12-19 nm particles was 19.4 ±12.69 nm.h^{-1} (Table 1), which is above the typical range of GRs reported in the literature for a similar size class of 7-20 nm. The review by Yli-Juuti et al.

320   (2011) of GR$_{7-20}$, obtained at different measurement sites located in various environments, reports a yearly average of 6.66 ±3.41 nm.h^{-1} (19 values) . However, higher GRs have been observed for a coastal environment in Australia, with an average GR$_{7-20}$ of 19 nm.h^{-1}, (Modini et al., 2009) and for a polluted urban environment in Tecamac, with an 18 nm.h^{-1} average GR$_{3.7-25}$ (Iida et al., 2008). It is noteworthy that, at high altitudes, the conditions of spatially homogeneous air masses and a steady state, necessary to calculate a realistic growth rate, are not

325   verified since air masses are progressively advected to the site from lower altitudes. Thus the GRs that are reported here are "apparent" growth rates that may be overestimated due to the transport of particles that have already nucleated and grown at lower altitudes at the same time. Nevertheless, the particle GR calculated for the Maïdo

station is higher than the average GRs reported by Rose et al. (2015a) for the CHC station (7.62 nm.h^{-1}), Boulon et al. (2011a) for the Puy-de-Dôme station (6.20 nm.h^{-1}), and Venzac et al. (2008) for Nepal (1.8 nm.h^{-1}).

330   In our calculation, 19 events were not taken into account because of the special characteristics of the extreme value of GR. The beginning of the FNP was characterized by a clear verticality in the spectrum during the first hours of the event and the corresponding GR was generally very high (100 to 150 nm.h^{-1}) or negative. Figure 6 shows two examples of DMPS spectra belonging to this special class of growth rates. Most of them were observed in December (8 cases). Dal Maso (2002) and O'Dowd and De Leeuw (2007) obtained such values (100 nm.h^{-1}) at

335   Mace Head, a coastal site in western Ireland. They can be explained by the simultaneous transport of nucleated and already grown particles to the sampling site, from seaweed fields. In the case of coastal marine NPF events, the spatial homogeneity of the emission field is not verified, as for high altitude sites.

Figure 7 highlights a clear seasonal variation of GR$_{12-19}$, with the highest monthly averages in August (35 nm.h^{-1}) and the lowest in May (8.9 nm.h^{-1}). These variations of the GR differ from those reported in the literature for other

340   high altitude sites. Boulon et al. (2011a), did not find a significant seasonal pattern in the GR variation at the Puy de Dôme. In Chacaltaya, Rose et al. (2015a) showed that, ==on average, the GRs were enhanced during the wet period, which is not in agreement with the present study, as we find high medians during the dry period (22.82 nm.h^{-1} averaged from July to November).==

Formation rates were calculated for 12 and 2 nm particles when the GR$_{12-19}$ was available. The yearly average

345   nucleation rates J$_{12}$ and J$_{2}$ in Table 1 are respectively 0.931 ±1.15 and 1.53 ±2.06 cm^{-3}.s^{-1}. These formation rates are in the upper range of the values reported by Kulmala et al. (2004) from measurements performed in more than 100 locations in the boundary layer (J$_{3}$ = 0.01-10 cm^{-3}.s^{-1}). They are of the same order of magnitude as the ones reported for the CHC (1.02 and 1.90 cm^{-3}.s^{-1} for the wet and dry seasons respectively, (Rose et al., 2015a).

J$_{2}$ seasonal variation follows the J$_{12}$ seasonal variation (Fig. 8) but with higher values due to losses by coagulation

350   during the growth process. We observe a clear seasonal cycle with maximum values during the dry season, particularly between July and September (J$_{12}$ = 1.60 cm^{-3}.s^{-1} and J$_{2}$ = 2.39 cm^{-3}.s^{-1} respectively, averaged over 3 months). These observations are consistent with those reported for CHC, where J$_{2}$ were reported to be twice as high during the dry season as in the wet season (Rose et al., 2015a). The lowest values are obtained around the transition months of December, with J$_{12}$ = 0.32 cm^{-3}.s^{-1} and J$_{2}$ = 0.52 cm^{-3}.s^{-1} (averaged between November and

355   January), and April, with J$_{12}$ = 0.44 cm^{-3}.s^{-1} and J$_{2}$ = 0.66 cm^{-3}.s^{-1} (averaged between April to June). The seasonal variation of the growth rate reported in Figure 7 also shows highest values around August but the seasonal variation of nucleation rates shows features different from those of the GR. Formation rates reach their maxima slightly earlier in the dry season (July) than the growth rates, and the contrast between July-August-Sept and the rest of the year is also stronger. This indicates that the condensable vapours necessary for nucleating new particles might

360   not have exactly the same seasonal variation as the ones required for growing the newly formed particles. ==The peak in July is correlated to the Somalian phytoplankton bloom, which indicates a possible influence of a marine source on the NPF intensity during this month.== In addition, high particle formation and growth rates obtained in July-August do not coincide with the highest nucleation frequencies, suggesting that, during these months, NPF might be less frequent but occur in the form of stronger events.

365   Several factors have previously been reported to influence the seasonal variation of the NPF event frequency, GR, and nucleation rates; they include (i) the availability of condensable gases involved in the formation of new particles, (ii) the number concentration of pre-existing particles transported to the site and (iii) thermo-dynamical

properties of the atmosphere, such as radiation, temperature, and relative humidity. In the following sections, we will explore the seasonal variation of the last two factors (ii and iii).

4.4 Meteorological parameters and onset of NPF

A summary of incidental radiation, relative humidity, temperature and pressure monthly averages is available in Table A2. Austral seasons are reflected regarding both the daily averaged temperature and radiation represented on Figure 9a. It is important to note that radiation is highest between September and November (272.19 W.m^{-2} on average), coinciding with one period of high NPF frequency (Fig. 5), but not with the maximum frequency of occurrence (March to May), nor with any high values of the GR or J_2/J_{12} (Figs. 7 and 8). Hence, the availability of light for photochemistry is not the only parameter influencing the NPF frequency. The temperature averages are higher from November to April (14.02 °C). As mentioned earlier, this parameter can influence the VOC emissions (Yu et al., 2017) since it is a condition for vegetation development and the decomposition of organic matter. The seasonal temperature variations are similar to the seasonal variation of the NPF event frequency but opposite to the GR and J_2/J_{12} seasonal variations. The relative humidity values are typical of an inter-tropical island with peaks in summer, between December and March (76.79% on average), and the lowest values obtained in July and September. The low relative humidity is hence the only meteorological parameter that seems to be related to the July-August-Sept nucleation rate peak. Figure 9b shows that the time of the nucleation onset seasonal variation is well correlated to the sunrise. During the southern summer, NPF starts between approximately 08:00 and 10:00 LT and between 09:00 and 10:00 during the southern winter. This correlation may be due to the need for sunlight to be available to start photochemical processes, or/and to the start of advection of precursor gases from lower altitude sources in the BL.

4.5 Condensation sink

In addition to the meteorological parameters, the seasonal variation of the NPF characteristics might also be influenced by the presence of pre-existing particles, known to inhibit the NPF processes by increasing the competition for available condensable gases. We averaged the CS for two hours before the nucleation started (CS$_2$) to properly characterize its influence on the occurrence of an NPF event. In Figure 9b, nucleation onset times are averaged for each season (08:00 LT for southern summer and 09:00 LT for southern winter). The yearly average condensation sink has been calculated to be 2.43 ×10^{-3} s^{-1} and 1.86 ×10^{-3} s^{-1} for CS$_2$. These values are similar to the ones reported for the altitude station of Chacaltaya (Rose et al., 2015a) and Nepal (Venzac et al., 2008) which are 2.4 ×10^{-3} s^{-1} and 2.1 ×10^{-3} s^{-1} respectively and also for the Mace Head coastal station (Dal Maso, 2002) which is about 2 × 10^{-3} s^{-1}.

Monthly averages of the CS$_2$ were calculated for event days and non-event days and are shown for 2015 on Figure 10, together with the NPF event monthly frequency, f_m. This representation highlights monthly averaged CS$_2$ peaks for February (2.65 ×10^{-3} s^{-1}), May (3.74 ×10^{-3} s^{-1}) and September (4.72 ×10^{-3} s^{-1}). The September value is similar to the South African savannah yearly average (Vakkari et al., 2011), which was about 4.3 ×10^{-3} s^{-1}. It attests to a considerable presence of pre-existing particles at the Maïdo station for this period. However, the NPF frequency seasonal pattern does not match that of low CS$_2$. May and September CS$_2$ peaks are associated with f_m peak values while January and June CS$_2$ low averages (0.89 and 0.96 ×10^{-3} s^{-1} respectively) are correlated to weak NPF occurrence.

Moreover, we calculated that the annual CS_{2ev} (event) median (1.2×10^{-3} s^{-1}) was significantly higher than the annual CS_{2noev} (no event) median (8.5×10^{-4} s^{-1}). The previous observations thus suggest that the condensation sink does not inhibit NPF at Maïdo, as previously reported for other high altitude stations (Manninen et al., 2010; Boulon et al., 2010; Rose et al., 2015b). At these sites, the occurrence of the NPF process might be determined

410   rather by the availability of condensable vapours, which are likely to be transported together with pre-existing particles from lower altitudes. Furthermore, we evaluated whether the frequency of nucleation was correlated to a frequency of exceeding a CS threshold. Hence, we calculated a monthly average frequency for which the CS_2 exceeded a threshold value of 1.04×10^{-3} s^{-1}. The threshold was chosen arbitrarily as a value intermediate between the annual CS_{2ev} and CS_{2noev} medians. The resulting frequency at which CS_2 exceeded the threshold (Fig. 11) had

415   a clear seasonal variation with maxima during the austral off-season periods. For April-May, and September-November, more than 60% of the CS_2 were higher than 1.04×10^{-3} s^{-1}, while for January, June and July the frequency was lowest. Hence, we actually find a positive correlation between the frequency of CS exceeding a threshold value and the frequency of occurrence of NPF events.

5 Conclusion

420   In the present study, we respond to the lack of NPF observations for both altitude and coastal sites in the southern hemisphere. We report the remarkably high frequency of occurrence of NPF events at the Maïdo observatory (65%). We also observe that there is a bimodal seasonal variation of this frequency, characterized by high values during the austral off-season periods. We show that the condensation sink exceeds a threshold value (1.04×10^{-3} s^{-1}) with a similar seasonal variation of frequency, suggesting that, similarly to other altitude sites, the condensation

425   sink does not inhibit NPF at Maïdo, but the occurrence of the NPF process might be determined rather by the availability of condensable vapours, which are likely to be transported together with pre-existing particles from lower altitudes. In fact, temperatures have a seasonal variation that correspond to the seasonal variations of the NPF frequency of occurrence, and radiation is also highest during the spring maximum frequency of occurrence, but not during the autumn maximum. Temperatures may have an indirect link to NPF via their effect on BVOC

430   emissions. Finally, CO, a possible indicator of a stronger anthropogenic influence, also has a maximum during the austral spring season. The seasonal variations of the nucleation rate and growth rate are not correlated to the NPF frequency seasonal variation. Nucleation rates and growth rates are maximal during the dry season, corresponding to low relative humidity conditions, but also to the Somalian phytoplankton bloom (July). While annual average J_{12} and J_2 are in the typical ranges found in the literature ($9.31 \times 10^{-2} \pm 1.15$ and 1.53 ± 2.06 cm^{-3}.s^{-1} respectively),

435   GR_{12-19} values are higher than the typical range of GRs reported in the literature (19.4 ± 12.69 nm.h^{-1}). We also distinguish 19 specific events with very high GR values that are in the range of GR observed at a coastal site in western Ireland. Essentially, the seasonal variation of the NPF event frequency, GR, and nucleation rates can be influenced by the seasonal variation of several gas-phase precursor sources. At Reunion Island, the secondary emissions assessment is not established and sources are not well-identified. It would be necessary to clearly locate

440   potential emission areas and estimate ultra-fine particle concentration fluxes for these different sources, such as vegetation or marine sources. In addition and although they are complex, modelling methods should be used to understand the origin of the local air masses and source contributions at the Maïdo observatory.

Acknowledgments

This project has received funding from the European Union's Horizon 2020 research and innovation programme
445   under grant agreement No 654109 (ACTRIS-2), from the French programme SNO-CLAP, and from the
OMNCG/OSU-R programme of La Réunion University. We also wish to thank the ORA (Observatoire
Réunionnais de l'Air) for providing the SO_2 dataset.

References

Almeida, J., Downard, A. J., Flagan, R. C. and Seinfeld, J. H.: Molecular understanding of sulphuric
450   acid–amine particle nucleation in the atmosphere, Nature, 502(7471), 359–363, 2013.

Baldy, S., Ancellet, G., Bessafi, M., Badr, A. and Luk, D. L. S.: Field observations of the vertical
distribution of tropospheric ozone at the island of Reunion (southern tropics), J. Geophys. Res.
Atmospheres, 101(D19), 23835–23849, doi:10.1029/95JD02929, 1996.

Baray, J.-L., Courcoux, Y., Keckhut, P., Portafaix, T., Tulet, P., Cammas, J.-P., Hauchecorne, A., Godin-
455   Beekmann, S., De Mazière, M., Hermans, C. and others: Maïdo observatory: a new high-altitude
station facility at Reunion Island (21° S, 55° E) for long-term atmospheric remote sensing and in situ
measurements, Atmospheric Meas. Tech., 6(10), 2865–2877, 2013.

Bates, T. S., Kapustin, V. N., Quinn, P. K., Covert, D. S., Coffman, D. J., Mari, C., Durkee, P. A., De
Bruyn, W. J. and Saltzman, E. S.: Processes controlling the distribution of aerosol particles in the
460   lower marine boundary layer during the First Aerosol Characterization Experiment (ACE 1), J.
Geophys. Res. Atmospheres, 103(D13), 16369–16383, doi:10.1029/97JD03720, 1998.

Bianchi, F., Tröstl, J., Junninen, H., Frege, C., Henne, S., Hoyle, C. R., Molteni, U., Herrmann, E.,
Adamov, A., Bukowiecki, N. and others: New particle formation in the free troposphere: A question
of chemistry and timing, Science, 352(6289), 1109–1112, 2016.

465   Bonn, B., Kulmala, M., Riipinen, I., Sihto, S.-L. and Ruuskanen, T. M.: How biogenic terpenes govern
the correlation between sulfuric acid concentrations and new particle formation, J. Geophys. Res.
Atmospheres, 113(D12) [online] Available from:
http://onlinelibrary.wiley.com/doi/10.1029/2007JD009327/full (Accessed 24 August 2017), 2008.

Boulon, J., Sellegri, K., Venzac, H., Picard, D., Weingartner, E., Wehrle, G., Collaud Coen, M.,
470   Bütikofer, R., Flückiger, E., Baltensperger, U. and Laj, P.: New particle formation and ultrafine charged
aerosol climatology at a high altitude site in the Alps (Jungfraujoch, 3580 m a.s.l., Switzerland),
Atmospheric Chem. Phys., 10(19), 9333–9349, doi:10.5194/acp-10-9333-2010, 2010.

Boulon, J., Sellegri, K., Hervo, M., Picard, D., Pichon, J.-M., Fréville, P. and Laj, P.: Investigation of
nucleation events vertical extent: a long term study at two different altitude sites, Atmospheric
475   Chem. Phys., 11(12), 5625–5639, doi:10.5194/acp-11-5625-2011, 2011a.

Boulon, J., Sellegri, K., Hervo, M. and Laj, P.: Observations of nucleation of new particles in a volcanic
plume, Proc. Natl. Acad. Sci., 108(30), 12223–12226, 2011b.

Boy, M., Kulmala, M., Ruuskanen, T. M., Pihlatie, M., Reissell, A., Aalto, P. P., Keronen, P., Maso, M.
D., Hellen, H., Hakola, H. and others: Sulphuric acid closure and contribution to nucleation mode
480   particle growth, Atmospheric Chem. Phys., 5(4), 863–878, 2005.

Clain, G., Baray, J.-L., Delmas, R., Diab, R., Leclair De Bellevue, J., Keckhut, P., Posny, F., Metzger, J.-M. and Cammas, J.-P.: Tropospheric ozone climatology at two Southern Hemisphere tropical/subtropical sites, (Reunion Island and Irene, South Africa) from ozonesondes, LIDAR, and in situ aircraft measurements, Atmospheric Chem. Phys., 9(5), 1723–1734, doi:10.5194/acp-9-1723-2009, 2009.

485 D O'Dowd, C. and De Leeuw, G.: Marine aerosol production: a review of the current knowledge, Philos. Trans. R. Soc. Lond. Math. Phys. Eng. Sci., 365(1856), 1753–1774, 2007.

Dal Maso, M.: Condensation and coagulation sinks and formation of nucleation mode particles in coastal and boreal forest boundary layers, J. Geophys. Res., 107(D19), doi:10.1029/2001JD001053, 2002.

490 Dal Maso, M., Kulmala, M., Riipinen, I., Wagner, R., Hussein, T., Aalto, P. P. and Lehtinen, K. E.: Formation and growth of fresh atmospheric aerosols: eight years of aerosol size distribution data from SMEAR II, Hyytiala, Finland, Boreal Environ. Res., 10(5), 323, 2005.

Duflot, V., Dils, B., Baray, J. L., De Mazière, M., Attié, J. L., Vanhaelewyn, G., Senten, C., Vigouroux, C., Clain, G. and Delmas, R.: Analysis of the origin of the distribution of CO in the subtropical southern 495 Indian Ocean in 2007, J. Geophys. Res. Atmospheres, 115(D22), D22106, doi:10.1029/2010JD013994, 2010.

Ehn, M., Thornton, J. A., Kleist, E., Sipilä, M. and Junninen, H.: A large source of low-volatility secondary organic aerosol, Nature, 27th February, 20, 2014.

Gale, E. F.: The production of amines by bacteria: The decarboxylation of amino-acids by strains of 500 Bacterium coli, Biochem. J., 34(3), 392, 1940.

Ge, X., Wexler, A. S. and Clegg, S. L.: Atmospheric amines – Part II. Thermodynamic properties and gas/particle partitioning, Atmos. Environ., 45(3), 561–577, doi:10.1016/j.atmosenv.2010.10.013, 2011.

Hallar, A. G., Petersen, R., McCubbin, I. B., Lowenthal, D., Lee, S., Andrews, E. and Yu, F.: Climatology 505 of New Particle Formation and Corresponding Precursors at Storm Peak Laboratory, Aerosol Air Qual. Res., 16(3), 816–826, doi:10.4209/aaqr.2015.05.0341, 2016.

Hamburger, T., McMeeking, G., Minikin, A., Birmili, W., Dall'Osto, M., O'Dowd, C., Flentje, H., Henzing, B., Junninen, H., Kristensson, A., de Leeuw, G., Stohl, A., Burkhart, J. F., Coe, H., Krejci, R. and Petzold, A.: Overview of the synoptic and pollution situation over Europe during the EUCAARI-510 LONGREX field campaign, Atmospheric Chem. Phys., 11(3), 1065–1082, doi:10.5194/acp-11-1065-2011, 2011.

Hirsikko, A., Laakso, L., Hõrrak, U., Aalto, P. P., Kerminen, V. and Kulmala, M.: Annual and size dependent variation of growth rates and ion concentrations in boreal forest, Boreal Environ. Res., 10(5), 357, 2005.

515 Hirsikko, A., Vakkari, V., Tiitta, P., Manninen, H. E., Gagné, S., Laakso, H., Kulmala, M., Mirme, A., Mirme, S., Mabaso, D., Beukes, J. P. and Laakso, L.: Characterisation of sub-micron particle number concentrations and formation events in the western Bushveld Igneous Complex, South Africa, Atmospheric Chem. Phys., 12(9), 3951–3967, doi:10.5194/acp-12-3951-2012, 2012.

Hutchinson, G. L., Mosier, A. R. and Andre, C. E.: Ammonia and Amine Emissions from a Large Cattle 520 Feedlot, J. Environ. Qual., 11(2), 288–293, doi:10.2134/jeq1982.00472425001100020028x, 1982.

Hyvönen, S., Junninen, H., Laakso, L., Dal Maso, M., Grönholm, T., Bonn, B., Keronen, P., Aalto, P., Hiltunen, V., Pohja, T., Launiainen, S., Hari, P., Mannila, H. and Kulmala, M.: A look at aerosol formation using data mining techniques, Atmos Chem Phys, 5(12), 3345–3356, doi:10.5194/acp-5-3345-2005, 2005.

525 Iida, K., Stolzenburg, M. R., McMurry, P. H. and Smith, J. N.: Estimating nanoparticle growth rates from size-dependent charged fractions: Analysis of new particle formation events in Mexico City, J. Geophys. Res. Atmospheres, 113(D5) [online] Available from: http://onlinelibrary.wiley.com/doi/10.1029/2007JD009260/full (Accessed 25 August 2017), 2008.

Kerminen, V.-M. and Kulmala, M.: Analytical formulae connecting the "real" and the "apparent"
530 nucleation rate and the nuclei number concentration for atmospheric nucleation events, J. Aerosol Sci., 33(4), 609–622, doi:10.1016/S0021-8502(01)00194-X, 2002.

Kesselmeier, J. and Staudt, M.: Biogenic Volatile Organic Compounds (VOC): An Overview on Emission, Physiology and Ecology, J. Atmospheric Chem., 33(1), 23–88, doi:10.1023/A:1006127516791, 1999.

535 Kirkby, J., Duplissy, J., Sengupta, K., Frege, C., Gordon, H., Williamson, C., Heinritzi, M., Simon, M., Yan, C., Almeida, J., Tröstl, J., Nieminen, T., Ortega, I. K., Wagner, R., Adamov, A., Amorim, A., Bernhammer, A.-K., Bianchi, F., Breitenlechner, M., Brilke, S., Chen, X., Craven, J., Dias, A., Ehrhart, S., Flagan, R. C., Franchin, A., Fuchs, C., Guida, R., Hakala, J., Hoyle, C. R., Jokinen, T., Junninen, H., Kangasluoma, J., Kim, J., Krapf, M., Kürten, A., Laaksonen, A., Lehtipalo, K., Makhmutov, V., Mathot,
540 S., Molteni, U., Onnela, A., Peräkylä, O., Piel, F., Petäjä, T., Praplan, A. P., Pringle, K., Rap, A., Richards, N. A. D., Riipinen, I., Rissanen, M. P., Rondo, L., Sarnela, N., Schobesberger, S., Scott, C. E., Seinfeld, J. H., Sipilä, M., Steiner, G., Stozhkov, Y., Stratmann, F., Tomé, A., Virtanen, A., Vogel, A. L., Wagner, A. C., Wagner, P. E., Weingartner, E., Wimmer, D., Winkler, P. M., Ye, P., Zhang, X., Hansel, A., Dommen, J., Donahue, N. M., Worsnop, D. R., Baltensperger, U., Kulmala, M., Carslaw, K. S. and Curtius, J.: Ion-
545 induced nucleation of pure biogenic particles, Nature, 533(7604), 521–526, doi:10.1038/nature17953, 2016.

Koponen, I. K., Virkkula, A., Hillamo, R., Kerminen, V.-M. and Kulmala, M.: Number size distributions and concentrations of the continental summer aerosols in Queen Maud Land, Antarctica, J. Geophys. Res. Atmospheres, 108(D18) [online] Available from:
550 http://onlinelibrary.wiley.com/doi/10.1029/2003JD003614/full (Accessed 24 August 2017), 2003.

Kulmala, M.: ATMOSPHERIC SCIENCE: How Particles Nucleate and Grow, Science, 302(5647), 1000–1001, doi:10.1126/science.1090848, 2003.

Kulmala, M. and Kerminen, V.-M.: On the formation and growth of atmospheric nanoparticles, Atmospheric Res., 90(2–4), 132–150, doi:10.1016/j.atmosres.2008.01.005, 2008.

555 Kulmala, M., Vehkamäki, H., Petäjä, T., Dal Maso, M., Lauri, A., Kerminen, V.-M., Birmili, W. and McMurry, P. H.: Formation and growth rates of ultrafine atmospheric particles: a review of observations, J. Aerosol Sci., 35(2), 143–176, doi:10.1016/j.jaerosci.2003.10.003, 2004.

Kulmala, M., Riipinen, I., Sipilä, M., Manninen, H. E., Petäjä, T., Junninen, H., Maso, M. D., Mordas, G., Mirme, A., Vana, M., Hirsikko, A., Laakso, L., Harrison, R. M., Hanson, I., Leung, C., Lehtinen, K. E. J.
560 and Kerminen, V.-M.: Toward Direct Measurement of Atmospheric Nucleation, Science, 318(5847), 89–92, doi:10.1126/science.1144124, 2007.

Kulmala, M., Kontkanen, J., Junninen, H., Lehtipalo, K., Manninen, H. E., Nieminen, T., Petäjä, T., Sipilä, M., Schobesberger, S., Rantala, P., Franchin, A., Jokinen, T., Järvinen, E., Äijälä, M.,

565 Kangasluoma, J., Hakala, J., Aalto, P. P., Paasonen, P., Mikkilä, J., Vanhanen, J., Aalto, J., Hakola, H., Makkonen, U., Ruuskanen, T., Mauldin, R. L., Duplissy, J., Vehkamäki, H., Bäck, J., Kortelainen, A., Riipinen, I., Kurtén, T., Johnston, M. V., Smith, J. N., Ehn, M., Mentel, T. F., Lehtinen, K. E. J., Laaksonen, A., Kerminen, V.-M. and Worsnop, D. R.: Direct Observations of Atmospheric Aerosol Nucleation, Science, 339(6122), 943–946, doi:10.1126/science.1227385, 2013.

570 Lehtinen, K. E. J., Dal Maso, M., Kulmala, M. and Kerminen, V.-M.: Estimating nucleation rates from apparent particle formation rates and vice versa: Revised formulation of the Kerminen–Kulmala equation, J. Aerosol Sci., 38(9), 988–994, doi:10.1016/j.jaerosci.2007.06.009, 2007.

Lesouëf, D., Gheusi, F., Delmas, R. and Escobar, J.: Numerical simulations of local circulations and pollution transport over Reunion Island, Ann. Geophys., 29(1), 53–69, doi:10.5194/angeo-29-53-2011, 2011.

575 Mäkelä, J. M., Riihelä, M., Ukkonen, A., Jokinen, V. and Keskinen, J.: Comparison of mobility equivalent diameter with Kelvin-Thomson diameter using ion mobility data, J. Chem. Phys., 105(4), 1562–1571, doi:10.1063/1.472017, 1996.

Makkonen, R., Asmi, A., Kerminen, V.-M., Boy, M., Arneth, A., Hari, P. and Kulmala, M.: Air pollution control and decreasing new particle formation lead to strong climate warming, Atmospheric Chem.
580 Phys., 12(3), 1515–1524, doi:10.5194/acp-12-1515-2012, 2012.

Manninen, H. E., Nieminen, T., Asmi, E., Gagné, S., Häkkinen, S., Lehtipalo, K., Aalto, P., Vana, M., Mirme, A., Mirme, S., Hõrrak, U., Plass-Dülmer, C., Stange, G., Kiss, G., Hoffer, A., Törő, N., Moerman, M., Henzing, B., de Leeuw, G., Brinkenberg, M., Kouvarakis, G. N., Bougiatioti, A., Mihalopoulos, N., O'Dowd, C., Ceburnis, D., Arneth, A., Svenningsson, B., Swietlicki, E., Tarozzi, L., Decesari, S., Facchini,
585 M. C., Birmili, W., Sonntag, A., Wiedensohler, A., Boulon, J., Sellegri, K., Laj, P., Gysel, M., Bukowiecki, N., Weingartner, E., Wehrle, G., Laaksonen, A., Hamed, A., Joutsensaari, J., Petäjä, T., Kerminen, V.-M. and Kulmala, M.: EUCAARI ion spectrometer measurements at 12 European sites – analysis of new particle formation events, Atmos Chem Phys, 10(16), 7907–7927, doi:10.5194/acp-10-7907-2010, 2010.

590 Martin, S. T., Andreae, M. O., Artaxo, P., Baumgardner, D., Chen, Q., Goldstein, A. H., Guenther, A., Heald, C. L., Mayol-Bracero, O. L., McMurry, P. H., Pauliquevis, T., Pöschl, U., Prather, K. A., Roberts, G. C., Saleska, S. R., Silva Dias, M. A., Spracklen, D. V., Swietlicki, E. and Trebs, I.: Sources and properties of Amazonian aerosol particles, Rev. Geophys., 48(2), RG2002, doi:10.1029/2008RG000280, 2010.

595 Mikkonen, S., Lehtinen, K. E., Hamed, A., Joutsensaari, J., Facchini, M. C. and Laaksonen, A.: Using discriminant analysis as a nucleation event classification method, Atmospheric Chem. Phys., 6(12), 5549–5557, 2006.

Mikkonen, S., Romakkaniemi, S., Smith, J. N., Korhonen, H., Petäjä, T., Plass-Duelmer, C., Boy, M., McMurry, P. H., Lehtinen, K. E. J., Joutsensaari, J., Hamed, A., Mauldin III, R. L., Birmili, W., Spindler,
600 G., Arnold, F., Kulmala, M. and Laaksonen, A.: A statistical proxy for sulphuric acid concentration, Atmospheric Chem. Phys., 11(21), 11319–11334, doi:10.5194/acp-11-11319-2011, 2011.

Modini, R. L., Ristovski, Z. D., Johnson, G. R., He, C., Surawski, N., Morawska, L., Suni, T. and Kulmala, M.: New particle formation and growth at a remote, sub-tropical coastal location, Atmospheric Chem. Phys., 9(19), 7607–7621, 2009.

605 National Institute of Statistical Economic Studies, INSEE: INSEE Conjoncture Réunion: Bilan économique 2016, 40p, [online] Available from: https://www.insee.fr/fr/statistiques/2856269, 2017.

Peltier, A., Beauducel, F., Villeneuve, N., Ferrazzini, V., Di Muro, A., Aiuppa, A., Derrien, A., Jourde, K. and Taisne, B.: Deep fluid transfer evidenced by surface deformation during the 2014–2015 unrest at Piton de la Fournaise volcano, J. Volcanol. Geotherm. Res., 321, 140–148,
610   doi:10.1016/j.jvolgeores.2016.04.031, 2016.

Petäjä, T., Mauldin Iii, R. L., Kosciuch, E., McGrath, J., Nieminen, T., Paasonen, P., Boy, M., Adamov, A., Kotiaho, T. and Kulmala, M.: Sulfuric acid and OH concentrations in a boreal forest site, Atmospheric Chem. Phys., 9(19), 7435–7448, 2009.

Pirjola, L., Kulmala, M., Wilck, M., Bischoff, A., Stratmann, F. and Otto, E.: Formation of Sulphuric Acid
615   Aerosols and Cloud Condensation Nuclei: An Expression for Significant Nucleation and Model Comprarison, J. Aerosol Sci., 30(8), 1079–1094, 1999.

Randriambelo, T., Baldy, S. and Bessafi, M.: The seasonality of ozone profile at Reunion Island: the role of biomass burning and of transport, in Geoscience and Remote Sensing, 1997. IGARSS '97. Remote Sensing - A Scientific Vision for Sustainable Development., 1997 IEEE International, vol. 1, pp.
620   6–8 vol.1., 1997.

Rastogi, N., Singh, A., Singh, D. and Sarin, M. M.: Chemical characteristics of PM2.5 at a source region of biomass burning emissions: Evidence for secondary aerosol formation, Environ. Pollut., 184, 563–569, doi:10.1016/j.envpol.2013.09.037, 2014.

Riccobono, F., Schobesberger, S., Scott, C. E., Dommen, J., Ortega, I. K., Rondo, L., Almeida, J.,
625   Amorim, A., Bianchi, F., Breitenlechner, M. and others: Oxidation products of biogenic emissions contribute to nucleation of atmospheric particles, Science, 344(6185), 717–721, 2014.

Rose, C., Sellegri, K., Velarde, F., Moreno, I., Ramonet, M., Weinhold, K., Krejci, R., Ginot, P., Andrade, M., Wiedensohler, A. and Laj, P.: Frequent nucleation events at the high altitude station of Chacaltaya (5240 m a.s.l.), Bolivia, Atmos. Environ., 102, 18–29,
630   doi:10.1016/j.atmosenv.2014.11.015, 2015a.

Rose, C., Sellegri, K., Velarde, F., Moreno, I., Ramonet, M., Weinhold, K., Krejci, R., Ginot, P., Andrade, M., Wiedensohler, A. and Laj, P.: Frequent nucleation events at the high altitude station of Chacaltaya (5240 m a.s.l.), Bolivia, Atmos. Environ., 102, 18–29, doi:10.1016/j.atmosenv.2014.11.015, 2015b.

635   Rose, C., Sellegri, K., Asmi, E., Hervo, M., Freney, E., Colomb, A., Junninen, H., Duplissy, J., Sipilä, M., Kontkanen, J., Lehtipalo, K. and Kulmala, M.: Major contribution of neutral clusters to new particle formation at the interface between the boundary layer and the free troposphere, Atmos Chem Phys, 15(6), 3413–3428, doi:10.5194/acp-15-3413-2015, 2015c.

Schade, G. W. and Crutzen, P. J.: Emission of aliphatic amines from animal husbandry and their
640   reactions: Potential source of N2O and HCN, J. Atmospheric Chem., 22(3), 319–346, 1995.

Schobesberger, S., Junninen, H., Bianchi, F., Lönn, G., Ehn, M., Lehtipalo, K., Dommen, J., Ehrhart, S., Ortega, I. K., Franchin, A., Nieminen, T., Riccobono, F., Hutterli, M., Duplissy, J., Almeida, J., Amorim, A., Breitenlechner, M., Downard, A. J., Dunne, E. M., Flagan, R. C., Kajos, M., Keskinen, H., Kirkby, J., Kupc, A., Kürten, A., Kurtén, T., Laaksonen, A., Mathot, S., Onnela, A., Praplan, A. P., Rondo, L.,
645   Santos, F. D., Schallhart, S., Schnitzhofer, R., Sipilä, M., Tomé, A., Tsagkogeorgas, G., Vehkamäki, H., Wimmer, D., Baltensperger, U., Carslaw, K. S., Curtius, J., Hansel, A., Petäjä, T., Kulmala, M., Donahue, N. M. and Worsnop, D. R.: Molecular understanding of atmospheric particle formation from sulfuric acid and large oxidized organic molecules, Proc. Natl. Acad. Sci., 110(43), 17223–17228, doi:10.1073/pnas.1306973110, 2013.

650   Seinfeld, J. H. and Pandis, S. N.: Atmospheric Chemistry and Physics: From Air Pollution to Climate Change, Third edition., John Wiley & Sons, New York., 2016.

Sellegri, K., Yoon, Y. J., Jennings, S. G., O'Dowd, C. D., Pirjola, L., Cautenet, S., Chen, H. and Hoffmann, T.: Quantification of Coastal New Ultra-Fine Particles Formation from In situ and Chamber Measurements during the BIOFLUX Campaign, Environ. Chem., 2(4), 260–270, doi:10.1071/EN05074,
655   2006.

Sellegri, K., Pey, J., Rose, C., Culot, A., DeWitt, H. L., Mas, S., Schwier, A. N., Temime-Roussel, B., Charriere, B., Saiz-Lopez, A., Mahajan, A. S., Parin, D., Kukui, A., Sempere, R., D'Anna, B. and Marchand, N.: Evidence of atmospheric nanoparticle formation from emissions of marine microorganisms, Geophys. Res. Lett., 43(12), 2016GL069389, doi:10.1002/2016GL069389, 2016.

660   Sihto, S.-L., Kulmala, M., Kerminen, V.-M., Maso, M. D., Petäjäī, T., Riipinen, I., Korhonen, H., Arnold, F., Janson, R., Boy, M. and others: Atmospheric sulphuric acid and aerosol formation: implications from atmospheric measurements for nucleation and early growth mechanisms, Atmospheric Chem. Phys., 6(12), 4079–4091, 2006.

Smith, J. N., Barsanti, K. C., Friedli, H. R., Ehn, M., Kulmala, M., Collins, D. R., Scheckman, J. H.,
665   Williams, B. J. and McMurry, P. H.: Observations of aminium salts in atmospheric nanoparticles and possible climatic implications, Proc. Natl. Acad. Sci., 107(15), 6634–6639, 2010.

Soler, O.: Atlas climatique de La Réunion (study report, 77p)., 2000.

Taupin, F. G., Bessafi, M., Baldy, S. and Bremaud, P. J.: Tropospheric ozone above the southwestern Indian Ocean is strongly linked to dynamical conditions prevailing in the tropics, J. Geophys. Res.
670   Atmospheres, 104(D7), 8057–8066, doi:10.1029/98JD02456, 1999.

Tulet, P. and Villeneuve, N.: Large scale modeling of the transport, chemical transformation and mass budget of the sulfur emitted during the April 2007 eruption of Piton de la Fournaise, Atmospheric Chem. Phys., 11(9), 4533–4546, doi:10.5194/acp-11-4533-2011, 2011.

Tulet, P., Di Muro, A., Colomb, A., Denjean, C., Duflot, V., Arellano, S., Foucart, B., Brioude, J., Sellegri,
675   K., Peltier, A., Aiuppa, A., Barthe, C., Bhugwant, C., Bielli, S., Boissier, P., Boudoire, G., Bourrianne, T., Brunet, C., Burnet, F., Cammas, J.-P., Gabarrot, F., Galle, B., Giudice, G., Guadagno, C., Jeamblu, F., Kowalski, P., Leclair de Bellevue, J., Marquestaut, N., Mékies, D., Metzger, J.-M., Pianezze, J., Portafaix, T., Sciare, J., Tournigand, A. and Villeneuve, N.: First results of the Piton de la Fournaise STRAP 2015 experiment: multidisciplinary tracking of a volcanic gas and aerosol plume, Atmos Chem
680   Phys, 17(8), 5355–5378, doi:10.5194/acp-17-5355-2017, 2017a.

Tulet, P., Di Muro, A., Colomb, A., Denjean, C., Duflot, V., Arellano, S., Foucart, B., Brioude, J., Sellegri, K., Peltier, A., Aiuppa, A., Barthe, C., Bhugwant, C., Bielli, S., Boissier, P., Boudoire, G., Bourrianne, T., Brunet, C., Burnet, F., Cammas, J.-P., Gabarrot, F., Galle, B., Giudice, G., Guadagno, C., Jeamblu, F., Kowalski, P., Leclair de Bellevue, J., Marquestaut, N., M?kies, D., Metzger, J.-M., Pianezze, J.,
685   Portafaix, T., Sciare, J., Tournigand, A. and Villeneuve, N.: First results of the Piton de la Fournaise STRAP 2015 experiment: multidisciplinary tracking of a volcanic gas and aerosol plume, Atmospheric Chem. Phys., 17(8), 5355–5378, doi:10.5194/acp-17-5355-2017, 2017b.

Turquet, J., Delesalle, B., Denis, M. and Blanchot, J.: Structure et dynamique du Phytoplancton côtier de La Réunion. Résultats de l'étude complémentaire (Programme PHYTO RUN.)., 2008.

690   Vakkari, V., Laakso, H., Kulmala, M., Laaksonen, A., Mabaso, D., Molefe, M., Kgabi, N. and Laakso, L.:
       New particle formation events in semi-clean South African savannah, Atmospheric Chem. Phys.,
       11(7), 3333–3346, doi:10.5194/acp-11-3333-2011, 2011.

       Veldhuis, M. J., Kraay, G. W., Van Bleijswijk, J. D. and Baars, M. A.: Seasonal and spatial variability in
       phytoplankton biomass, productivity and growth in the northwestern Indian Ocean: the southwest
695   and northeast monsoon, 1992–1993, Deep Sea Res. Part Oceanogr. Res. Pap., 44(3), 425–449, 1997.

       Venzac, H., Sellegri, K., Laj, P., Villani, P., Bonasoni, P., Marinoni, A., Cristofanelli, P., Calzolari, F.,
       Fuzzi, S., Decesari, S. and others: High frequency new particle formation in the Himalayas, Proc. Natl.
       Acad. Sci., 105(41), 15666–15671, 2008.

       Vigouroux, C., Stavrakou, T., Whaley, C., Dils, B., Duflot, V., Hermans, C., Kumps, N., Metzger, J.-M.,
700   Scolas, F., Vanhaelewyn, G., Müller, J.-F., Jones, D. B. A., Li, Q. and De Mazière, M.: FTIR time-series of
       biomass burning products (HCN, C_2H_6, C_2H_2, CH_3OH, and HCOOH) at Reunion Island (21° S,
       55° E) and comparisons with model data, Atmospheric Chem. Phys., 12(21), 10367–10385,
       doi:10.5194/acp-12-10367-2012, 2012.

       Wiedensohler, A., Birmili, W., Nowak, A., Sonntag, A., Weinhold, K., Merkel, M., Wehner, B., Tuch, T.,
705   Pfeifer, S., Fiebig, M., Fjäraa, A. M., Asmi, E., Sellegri, K., Depuy, R., Venzac, H., Villani, P., Laj, P.,
       Aalto, P., Ogren, J. A., Swietlicki, E., Williams, P., Roldin, P., Quincey, P., Hüglin, C., Fierz-
       Schmidhauser, R., Gysel, M., Weingartner, E., Riccobono, F., Santos, S., Grüning, C., Faloon, K.,
       Beddows, D., Harrison, R., Monahan, C., Jennings, S. G., O'Dowd, C. D., Marinoni, A., Horn, H.-G.,
       Keck, L., Jiang, J., Scheckman, J., Mcmurry, P. H., Deng, Z., Zhao, C. S., Moerman, M., Henzing, B., De
710   Leeuw, G., Löschau, G. and Bastian, S.: Mobility particle size spectrometers: harmonization of
       technical standards and data structure to facilitate high quality long-term observations of
       atmospheric particle number size distributions, Atmospheric Meas. Tech., 5, 657–685,
       doi:10.5194/amt-5-657-2012, 2012.

       Yli-Juuti, T., Nieminen, T., Hirsikko, A., Aalto, P. P., Asmi, E., Hõrrak, U., Manninen, H. E., Patokoski, J.,
715   Dal Maso, M., Petäjä, T., Rinne, J., Kulmala, M. and Riipinen, I.: Growth rates of nucleation mode
       particles in Hyytiälä during 2003−2009: variation with particle size, season, data analysis
       method and ambient conditions, Atmospheric Chem. Phys., 11(24), 12865–12886, doi:10.5194/acp-
       11-12865-2011, 2011.

       Yu, F., Wang, Z., Luo, G. and Turco, R.: Ion-mediated nucleation as an important global source of
720   tropospheric aerosols, Atmospheric Chem. Phys., 8(9), 2537–2554, 2008.

       Yu, F., Luo, G., Nadykto, A. B. and Herb, J.: Impact of temperature dependence on the possible
       contribution of organics to new particle formation in the atmosphere, Atmos Chem Phys, 17(8),
       4997–5005, doi:10.5194/acp-17-4997-2017, 2017.

Figures

725   **Figure 1: Map of Reunion Island and its location. Different terrain types are represented as well as a simplification of the local atmospheric dynamic pattern around the island.**
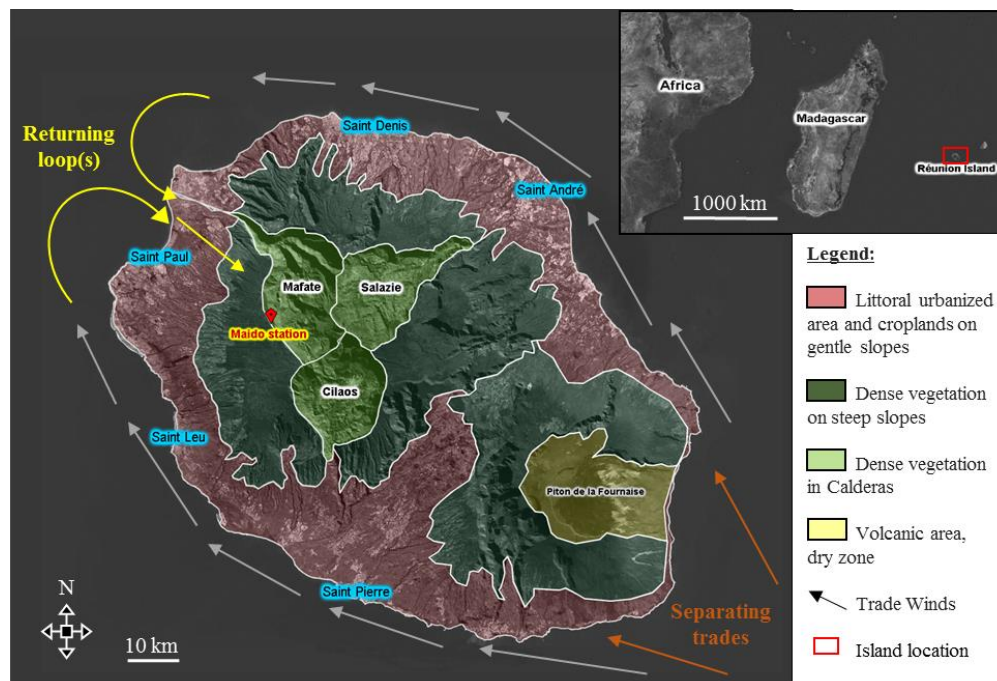
Figure 2: The annual variation of CO concentrations (ppb) in 2015 (daily averages).
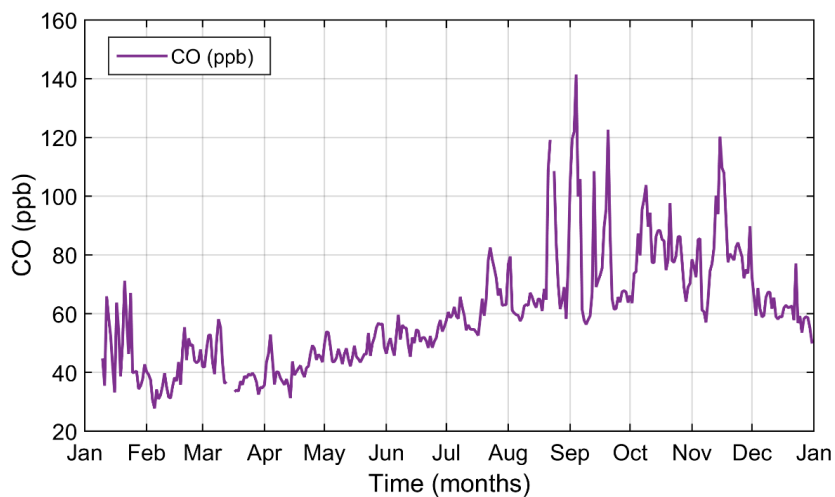
730   **Figure 3: Dataset from 2015 Maïdo campaign. Devices recorded data simultaneously from May to November.**
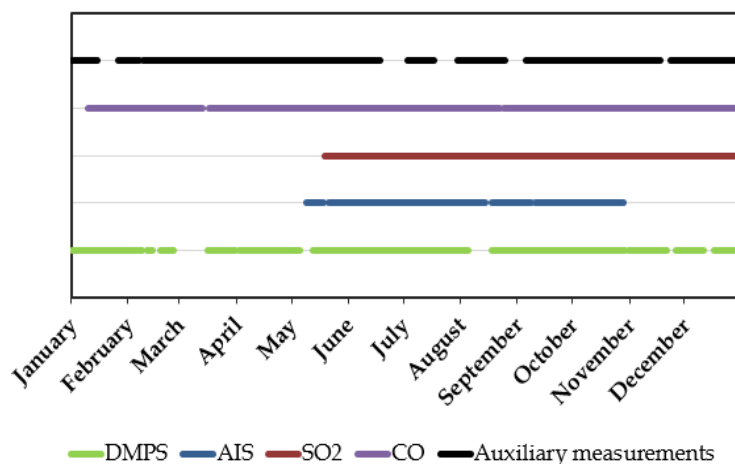
Figure 4: Negative ions (1-10 nm) and (10-700 nm) aerosol particle size distribution on 28 August 2015. Different colour scales are used as ion number concentrations measured with the AIS are lower than total particle number concentrations measured with the DMPS.
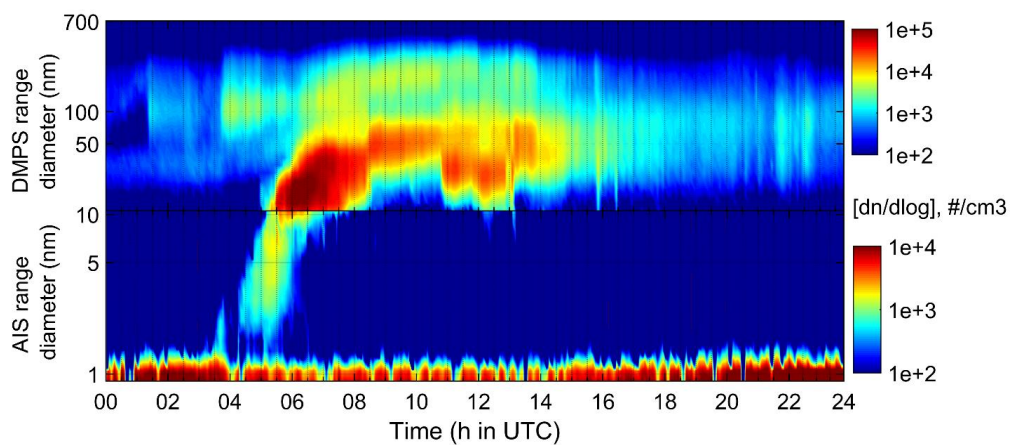
735

Figure 5: Monthly event frequency (%) variation during 2014 (green) and 2015 (blue). Values at the top of the bars correspond to the number of days that were taken in account for calculation.
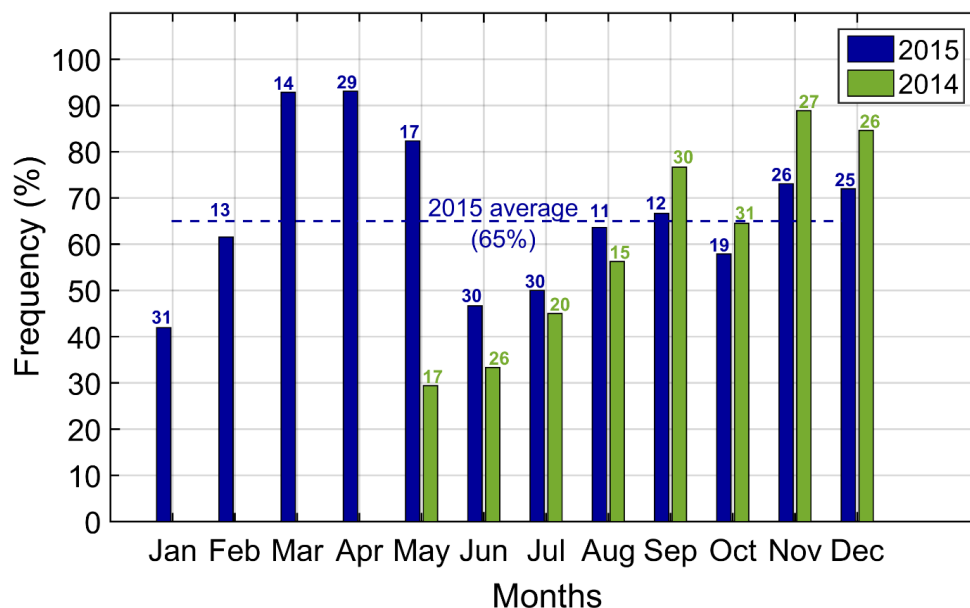
Figure 6: DMPS spectra for 31 January on the left and 25 March on the right. This is an evolution of the size distribution

740 **(left scale in nanometres) and of the aerosol concentration (colorimetric scale) with time (from 00 to 24 UTC).**
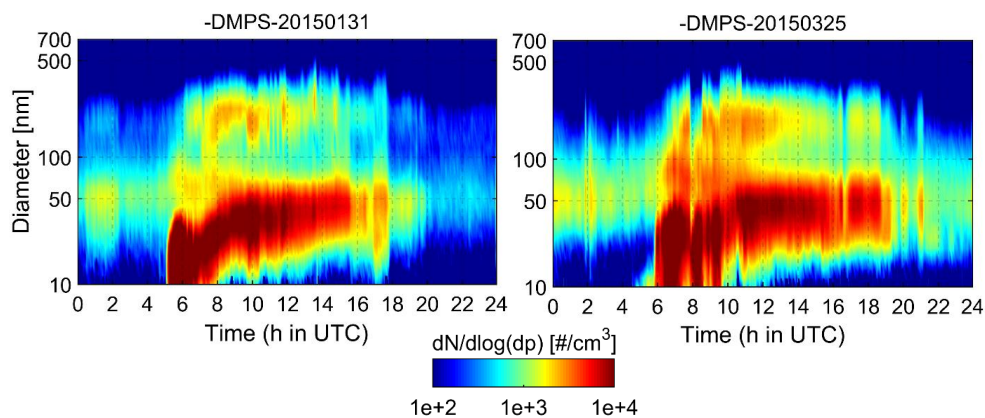
745 **Figure 7: Monthly median growth rates in 2015. Error bars in black represent 25ile (top) and 75ile (base). To build these representation, 146 growth rates were estimated on 167 days classified as event days.**
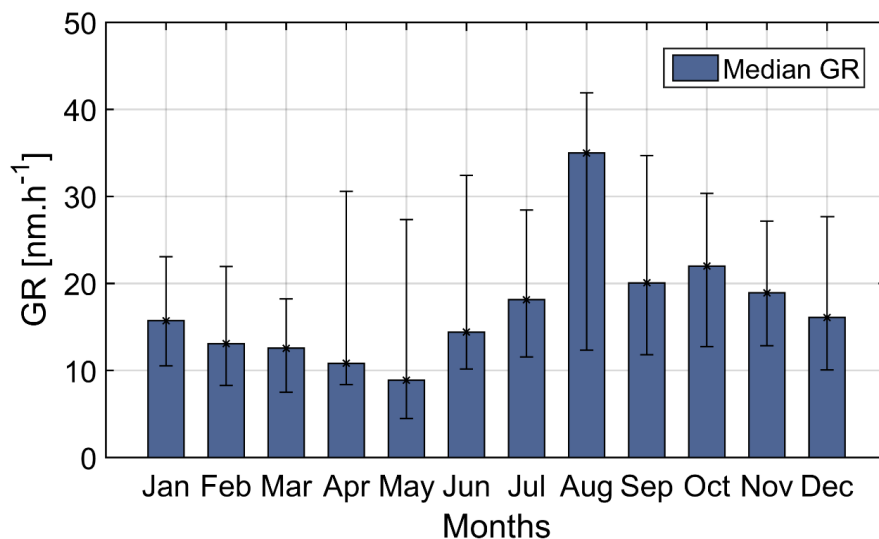
Figure 8: Monthly median nucleation rates in 2015 for 2 and 12 nm sizes. Error bars in black represent 25ile (top) and 75ile (base).
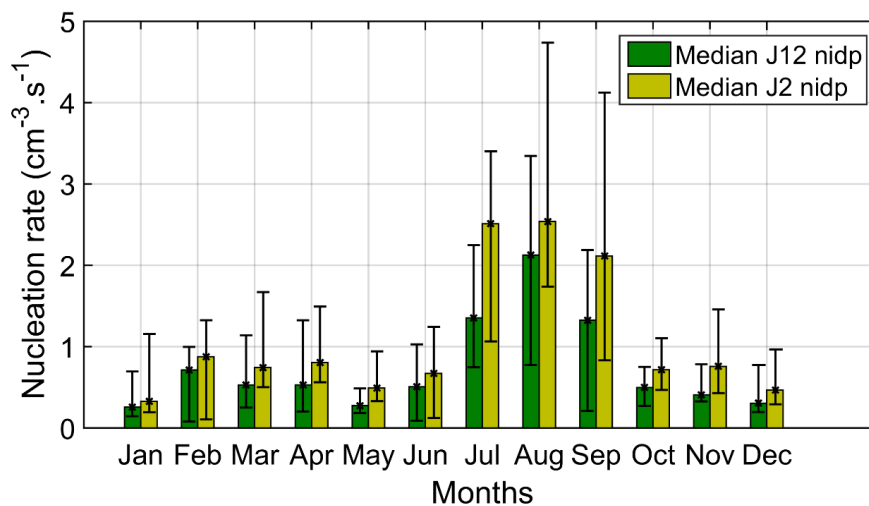
750

Figure 9: a) temperature (°C) and incidental radiation (W.m-2) variations during 2015 at Maïdo station given by daily UTC (fine) and monthly (bold) averages; b) seasonal variation of sunrise and time of NPF onset in UTC. The dry and the wet seasons are also delimited in orange and blue respectively.
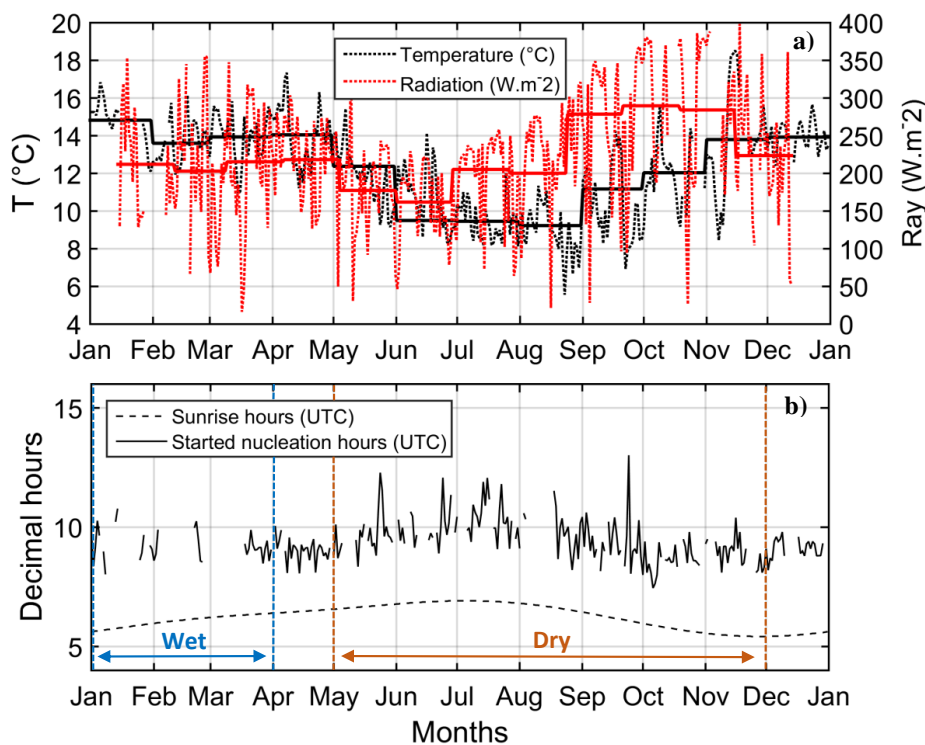
755   **Figure 10: Monthly CS_2 (blue) calculated two hours before NPF onset (scale at the right in s^{-1}) and monthly event frequency f_m (scale at the left in percentage). Averages have been calculated for event days (green), non-event days (red) and all days (blue).**
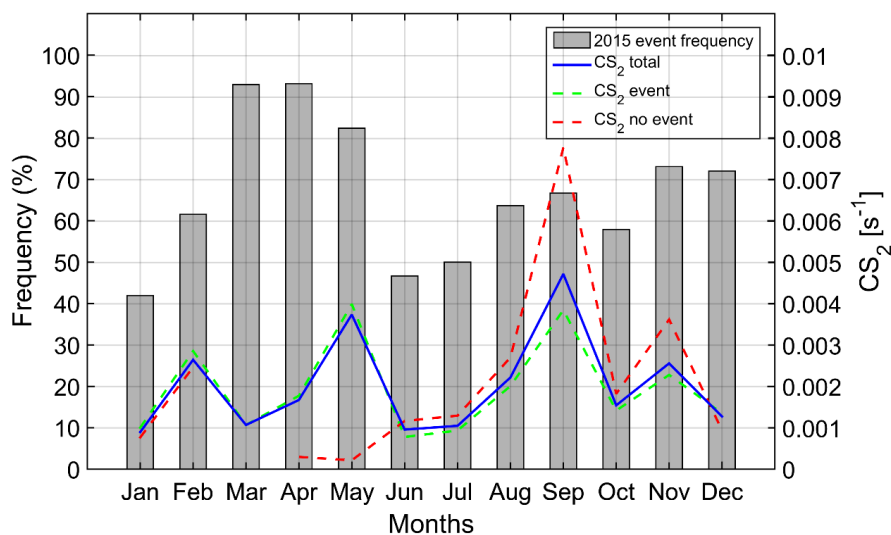
Figure 11: Monthly CS_2 proportion exceeding the average of CS_{2ev} and CS_{2noev} medians (1.04×10^{-3} s^{-1}).
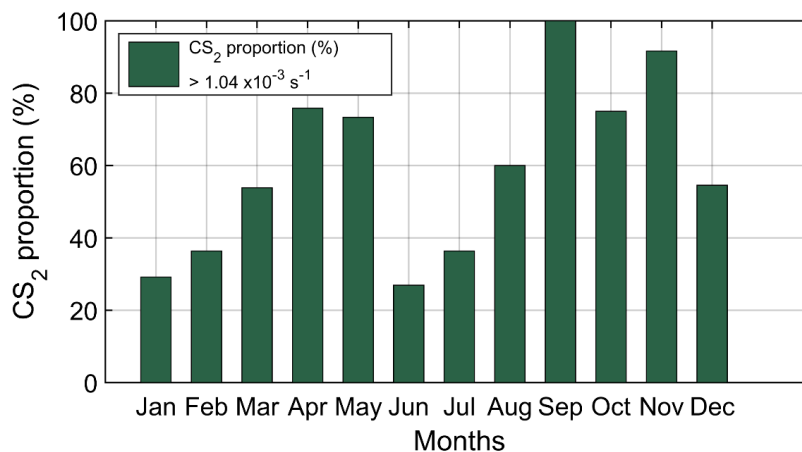
760

Table 1: Annual statistical values for $G_{12\text{-}19}$; J_{12}; J_2; CS and CS_2 calculated on daily averages.

	GR$_{12\_19}$ (nm.h^{-1})	J$_{12}$ (cm^{-3}.s^{-1})	J$_2$ (cm^{-3}.s^{-1})	CS (s^{-1})	CS$_2$ (s^{-1})
Averages	**19.455**	**0.931**	**1.531**	**2.43 ×10^{-3}**	**1.86 ×10^{-3}**
Standard dev.	12.689	1.153	0.920	2.06 ×10^{-3}	2.53 ×10^{-3}
Medians	**15.16**	**0.508**	**0.858**	**1.97 ×10^{-3}**	**1.15 ×10^{-3}**
25ile	9.58	0.223	0.385	1.19 ×10^{-3}	6.55 ×10^{-4}
75ile	27.69	1.131	1.756	2.96 ×10^{-3}	2.00 ×10^{-3}

Appendices

Figure A1: SO$_2$ concentration (ppb) at Maïdo station in 2015, showing the occurrence of three eruptive periods in red

765 **(17 to 30/05, 31/07 to 02/08 and 24/08 to 18/10)**
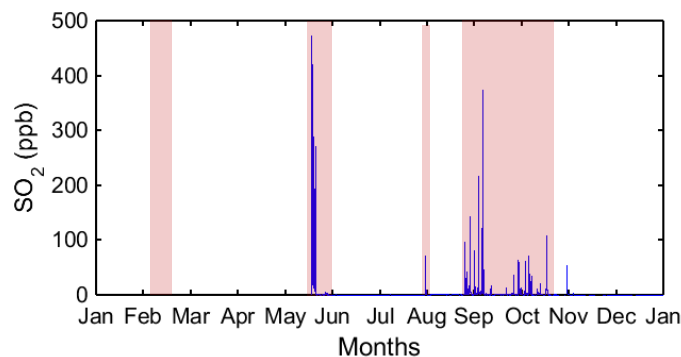
Sulfur dioxide concentrations allow us to distinguish days when NPF can be affected by the presence of the volcanic plume. Based on a 1 ppb threshold, which was the 97th percentile of the series, we considered that 47 days were plume days at the Maïdo station and removed them. The eruptive periods are clearly visible on this

770 figure.

Table A1: Meteorological parameter averages.

	Ray (W.m^{-2})	RH (%)	T (°C)	P (hPa)
January	212.07	78.77	14.82	787.21
February	202.98	77.17	13.60	788.85
March	215.42	74.11	13.93	789.45
April	218.26	66.70	14.05	789.41
May	177.43	72.20	12.38	791.51
June	161.91	70.00	9.50	790.90
July	205.30	53.78	9.46	792.52
August	200.18	64.46	9.23	791.93
September	278.64	50.02	11.17	791.02
October	289.73	63.55	12.04	791.92
November	248.20	56.26	13.80	789.91
December	223.63	77.10	13.92	790.16
Yearly average	**222.48**	**67.01**	**12.32**	**790.40**

Table A2: Comparison of NPF frequency, GR, J and CS values

Study	Location	Environment	NPF (%)	GR (nm.h^{-1})	J (cm^3.s^{-1})	CS (s^{-1})
Dal Maso (2002)	Ireland	Coastal	-	15 to 180	300 to 10000	2 ×10^{-3}
Koponen (2003)	Antarctica	Coastal	-	1 - 2	0.5	-
Iida (2008)	Mexico	Urban	-	18	1900 to 3000	-
McMurry (2003)	Atlanta, GA	Urban	-	2 – 6	20 to 70	-
Venzac (2008)	Nepal	Altitude	35%	2	< 0.2	2.1 ×10^{-3}
Modini (2009)	Australia	Coastal	65%	19	-	
Vakkari (2011)	South Africa	Remote, Altitude, Savannah	83%	8.9	0.5	4.3 ×10^{-3}
Boulon (2011)	France	Altitude	35.9%	6.20	1.382	3.7 ×10^{-3}
Rose (2015)	Bolivia	Altitude	63.9%	7.62	-	2.4 ×10^{-3}
Foucart (2017)	**Reunion**	**Coastal, Altitude**	**65%**	**GR$_{12-19}$ = 19.455**	**J$_{12}$ = 0.931, J$_2$ = 1.531**	**2.43 ×10^{-3}**

775

This table is given to help in the comparison of NPF parameters as a function of the different types of environments. A few stations are listed here. The values of the present study are summarized in the last line and the closest ones are highlighted (yellow). Reunion Island seems to present NPF characteristics of several environment types. The GRs and Js listed in the table are in a similar range to those estimated in the present study.

780

Figure A2: Diurnal variation of CS
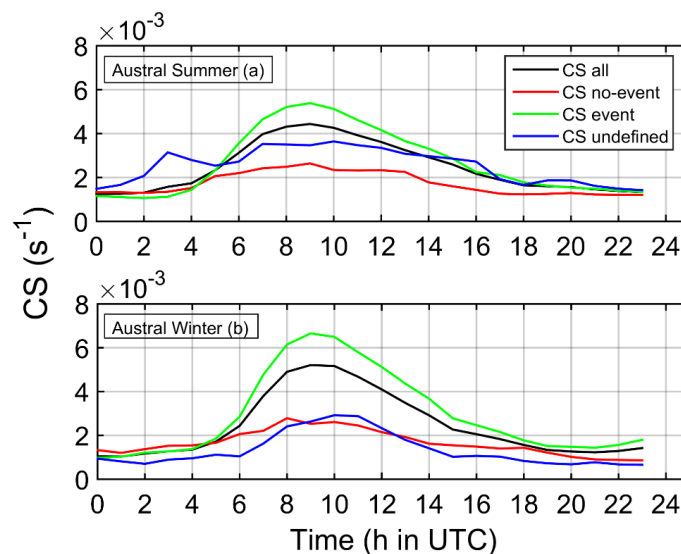
As the CS parameter varies throughout the day, we have also chosen to show the average daily variation of CS for summer a) and for winter b). Averages were calculated on undefined (CS_{un}), no-event (CS_{noev}), event (CS_{ev}) and all days. Maximum of CS all and CS_{ev} are reached at 9:00 UTC for both seasons but are higher for winter (CS_{all} = 5.1 ×10^{-3} s.$^{-1}$; CS_{ev} = 6.9 ×10^{-3} s^{-1}) than summer (CS_{all} = 4.5 ×10^{-3} s^{-1}; CS_{ev} = 5.2 ×10^{-3} s^{-1}). CS_{ev} really begins to increase at 4:00 UTC for summer but 5:00 UTC for winter. This corresponds to the moment when CS_{noev} becomes lower than CS_{ev}. Before these times, CS_{noev} is 10^{-4} higher than CS_{ev}, implying that CS_{noev} is too large to trigger new particle formation. Consequently, and thanks to this daily representation, we assume that CS affects the new particle formation trigger for both seasons in 2015. Moreover, it can be seen that CS_{un} curves follow the CS_{noev} curves better than CS_{ev} so it is possible that no-event days were not well recognized.

Figure A3: DMPS spectra for a) April and b) June months. We can clearly observe an event number difference between the two months according to the different FNP occurrence averages which are 93.1% for April and 46.7% for June.

795